OBLIQUE INTERACTION OF SOLITARY WAVES

MIN CHEN

Department of Mathematics, Purdue University,
West Lafayette, IN 47907, USA

Keywords: water wave, Boussinesq system, Legendre-Galerkin method, oblique interaction of solitary waves

Abstract. A highly efficient and accurate numerical scheme for initial and boundary value problems of a two-dimensional Boussinesq system which describes three-dimensional water waves is used to study in details the oblique interaction of a solitary wave and the evolution of solitary waves coming out of a narrower channel.

1. Introduction

A Boussinesq system which models surface water waves on a channel with bottom topography $\tilde{h}(x, y, t)$, which could be time-dependent, and with surface pressure variation $P(x, y, t)$ is used in this paper to investigate various wave phenomena. The general system reads

$$
\begin{aligned}
&\eta_t + \nabla \cdot \boldsymbol{v} + \nabla \cdot (h + \eta)\boldsymbol{v} - \frac{1}{6}\Delta\eta_t = F(h_{xxt}, h_{xtt}, \nabla P), \\
&\boldsymbol{v}_t + \nabla\eta + \frac{1}{2}\nabla|\boldsymbol{v}|^2 - \frac{1}{6}\Delta\boldsymbol{v}_t = G(h_{xxt}, h_{xtt}, \nabla P),
\end{aligned}
\tag{1.1}
$$

where $h = \frac{\tilde{h} - h_0}{h_0}$ with h_0 being the average water depth. The detailed derivation, justification and analysis of this system can be found in [4, 8, 5, 6]. It is worth to note that the fluid is bounded by the bottom topography $\tilde{h}(x, y, t)$ and the free surface $\eta(x, y, t)$ and $\eta(x, y, t)$ is a fundamental unknown of the problem. $\boldsymbol{v}(x, y, t)$ denotes the horizontal velocity field at height $\sqrt{\frac{2}{3}}h_0$.

Some of the advantages of this Boussinesq system when it is compared with the full Euler's equation include, the equations are posed on a fixed domain and the problem is no longer a moving boundary problem; η is an unknown function in the equation, not in the boundary condition; the unknown functions are with respect to (x, y, t), not (x, y, z, t), one less space dimension in the computation; the equations are regularized, and the boundary value problem is well posed. The three-dimensional velocity field at any other location (x, y, z) can be obtained by

$$\boldsymbol{u}(x,y,z,t) = (u,v) = (1+\frac{1}{2}(\frac{2}{3}-z^2)\Delta)\boldsymbol{v}(x,y,t),$$
$$w(x,y,z,t) = -z(1+\frac{1}{3}\Delta)\nabla\cdot\boldsymbol{v}(x,y,t).$$

It is noted that this is only one member of a class of Boussinesq systems. More references on Boussinesq systems can be found in [7, 16, 4, 13].

In this paper, we consider an L by H wave tank with flat bottom and constant air pressure at the water surface. The Boussinesq system (1.1) then has $F = G = 0$ and is valid on the domain $\Omega = (0, L) \times (0, H)$. Several physically relevant problems will be solved numerically.

The second-order semi-implicit Crank-Nicolson-leap-frog scheme (with the first step computed by a semi-implicit backward-Euler scheme) is used for time-discretization. At each time step, we only have to solve a sequence of Poisson type equations. For space discretization, various spectral method based numerical techniques are used depends on the types of the boundary conditions imposed. For periodic boundary conditions in the x-direction and Dirichlet boundary conditions in the y-direction, the Fourier-Chebyshev Galerkin method is used. In consequence, spectral accuracy is achieved and the total operation count is $O(NM\log(NM))$, where N and M are the number mode in x and y directions, which is quasi optimal. When Dirichlet boundary conditions are imposed on all four sides of the wave tank, the numerical simulation is more costly. It is worth to note that in general, boundary conditions on the four sides of the wave tank should be consistent at the four corners of the wave tank. Furthermore, the initial and boundary conditions should be consistent on where they intersect. The details of the scheme are described in [10].

2. Preservation of solitary waves with varying channel width

In this experiment, we study the evolution of a solitary wave coming out a narrow channel to a wider channel. Because the lack of exact, explicit solitary wave solutions for (1.1), the exact solution of one-way BBM equation [2] with amplitude A

$$\eta_0(x,t) = A sech^2(\sqrt{\frac{3A}{4K_0}}(x-K_0t) \tag{2.1}$$

withe $K_0 = 1 + \frac{A}{2}$ together with the first order approximation for velocity

$$v(x,t) = \eta(x,t) - \frac{\eta(x,t)^2}{4} \tag{2.2}$$

will be used for the initial conditions.

By following the work in [15, 1], the simulation starts from an approximate "line-soliton" spanning only half the width of the tank. It is noticed in paper [15], where numerical simulation was performed on the KP equation, a equation with additional assumptions that the wave is almost weakly three-dimensional and propagating predominantly in one-direction (see [14, 9] for detail), that after the initial disturbance is released, it bends backwards and slows down but, as soon as it feels the presence of the side wall, it quickly adjust to form a KdV (or one-dimensional) soliton with lower amplitude.

In this experiment, we take the width of channel to be 12 and the length to be 100, and let the initial data be

$$\begin{aligned}
&\eta(x,y,0) = \begin{cases} \operatorname{sech}^2(\sqrt{\frac{1}{2}} * (y-40)) & \text{for } 3 < x < 9, \\ 0 \quad \text{for other } x, \end{cases} \\
&v(x,y,0) = \eta(x,y,0) - \frac{\eta(x,y,0)^2}{4}, \\
&u(x,y,0) = 0.
\end{aligned} \tag{2.3}$$

The boundary data at two ends of the wave tank $y = 0$ and $y = 100$ are taken to be zero. The periodic boundary conditions are assumed on the sides of the wave tank ($x = 0$ and $x = 12$). It is worth to note that the middle section of the initial data (2.3) we choose here is not an exact solution of (1.1), but the exact solution of a one-dimensional Boussinesq equation associated with an approximate velocity field. But previous simulation show that it is quite close to a solitary wave solution of (1.1). If this initial data is imposed to span the whole width of the wave tank, which is equivalent to consider the one-dimensional solitary wave, it would develop into a solitary wave with height about 0.9 [3].

The solution $\eta(x,y,t)$ at $t = 0, 2, 5, 10, 20, 40$ are plotted in Figure 1 and Figure 2. The solitary wave first bends backward with a trough behind the leading wave. After it feels the boundary, it stretches and form a "clean" straight solitary wave span the whole channel. At $t = 40$, the tail part consists a traveling two-dimensional wave patten (a doubly periodic solution, see [11, 12] for more information) and a stationary tails. The qualitative behavior of the leading wave agrees with the observation described in [15] where the KP equation was used. There

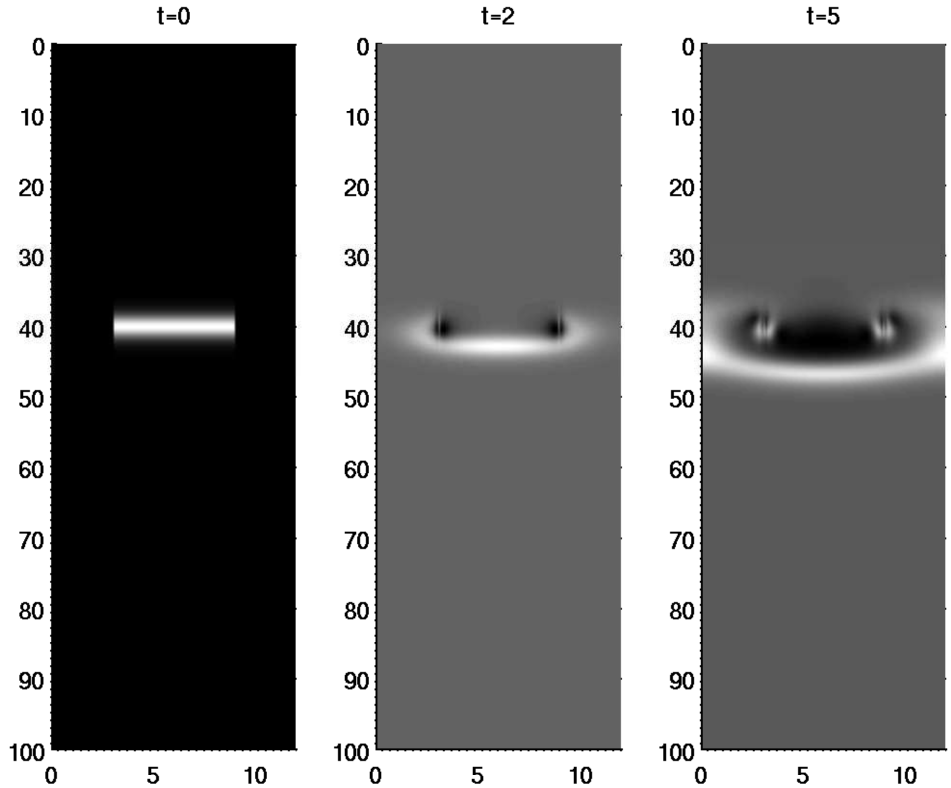

FIGURE 1. Simulation of a solitary wave initially spanning half width of the cannel and propagating to form a leading solitary wave spanning the whole width. The surface profiles at t=0, 2, 5 are plotted where light area are peaks and dark areas are troughs.

are also significant difference between the results of these two simulations. Instead of a relative clean soliton, we see a leading solitary wave followed by significant sized disturbances and the formation of a two-dimensional wave pattern.

In Figure 3, the function $\eta(6, y, 40)$ is plotted which shows that the height of the leading solitary wave is a much smaller (about 0.43) comparing to the initial wave because the widening of the cannel.

In summary, when a solitary wave comes out a narrower channel to a channel which is double the width, it develops into a smaller solitary wave, with about half (or a little smaller) of the original height and a structured tail wave.

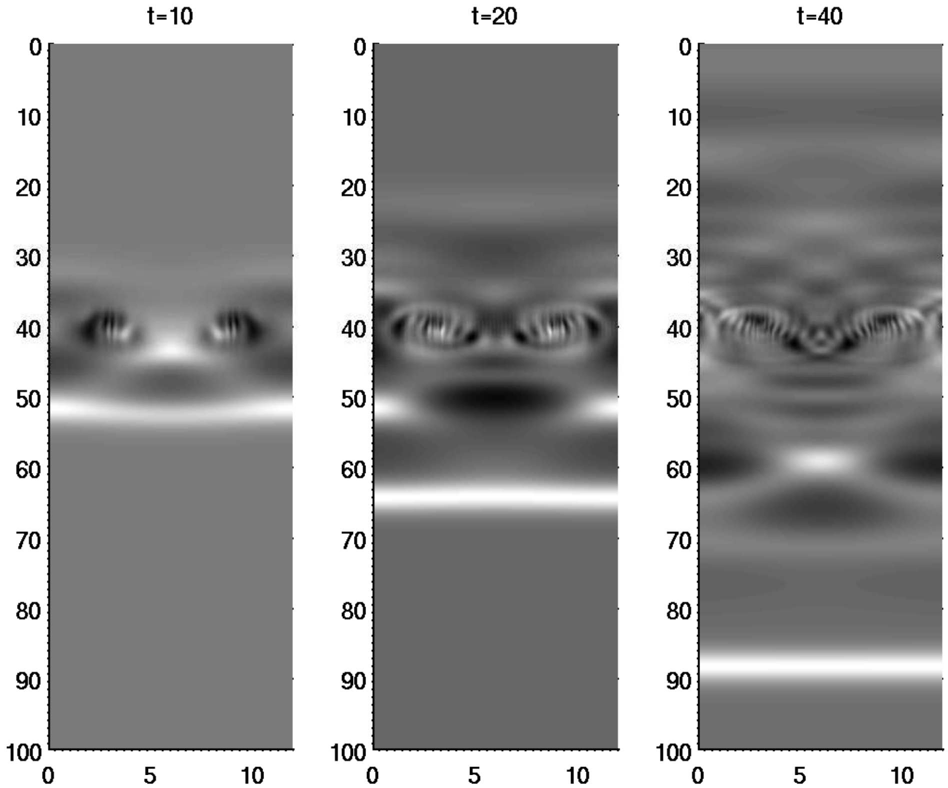

FIGURE 2. Continue from Figure 1 with surface profiles at t=10, 20, 40.

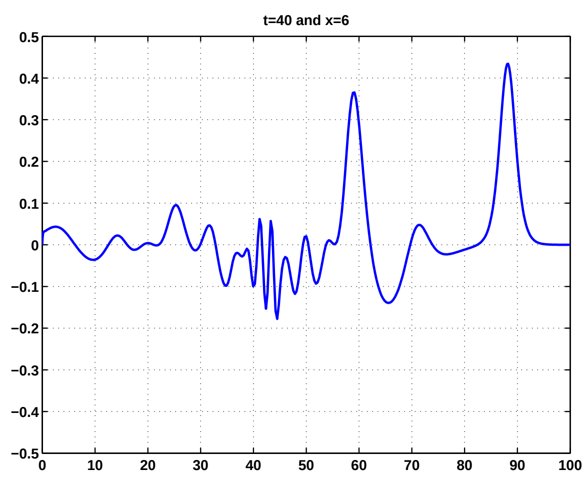

FIGURE 3. Wave surface at $x = 6$ and $t = 40$.

3. Oblique interactions of solitary waves

In this sequence of experiments, we start with two approximate solitary waves which form an oblique angle of θ and observe the oblique interaction of such two solitary waves.

Again, due to the lack of exact solitary solutions, the solution (2.1)-(2.2) with amplitude A will be used for the initial data. The initial data for the wave traveling down and right reads, where $\theta_1 = \frac{\theta}{2}$,

$$\begin{aligned} \eta(x,y,0) &= \eta_0\left(\frac{1}{\sqrt{1+tan^2(\theta_1)}}(\tan(\theta_1)x - y + y_0 - \frac{L}{2}\tan(\theta_1))\right), \\ u(x,y,0) &= -\frac{\tan(\theta_1)}{\sqrt{1+tan^2(\theta_1)}}(\eta(x,y,0) - \frac{1}{4}\eta^2(x,y,0)), \\ v(x,y,0) &= \frac{1}{\sqrt{1+tan^2(\theta_1)}}(\eta(x,y,0) - \frac{1}{4}\eta^2(x,y,0)), \end{aligned} \tag{3.1}$$

and the wave traveling down and left has the following form

$$\begin{aligned} \eta(x,y,0) &= \eta_0\left(\frac{1}{\sqrt{1+tan^2(\theta_1)}}(\tan(\theta_1)x + y - y_0 - \frac{L}{2}\tan(\theta_1))\right), \\ u(x,y,0) &= \frac{\tan(\theta_1)}{\sqrt{1+tan^2(\theta_1)}}(\eta(x,y,0) - \frac{1}{4}\eta^2(x,y,0)), \\ v(x,y,0) &= \frac{1}{\sqrt{1+tan^2(\theta_1)}}(\eta(x,y,0) - \frac{1}{4}\eta^2(x,y,0)). \end{aligned} \tag{3.2}$$

It is assumed that the solution is zero at the two ends of the wave tank and periodic on the sides of the wave tank.

We now study the oblique interaction of solitary waves in detail with respect to various attack angle θ.

3.1. $A = 0.2$ **and** $\theta = 40^o$**.** The first experiment is performed for initial data with $A = 0.2$, $\theta = 40^o$ and $y_0 = 40$. The computational domain is taken to be $[0, 200] \times [0, 180]$ with 512 modes in each direction and time-step being 0.025. The wave surfaces at $t = 0, 40, 80$ are plotted in Figure 4. The wave surface at $t = 0$ is the initial wave profile, which consists two solitary waves moving down. The solutions at times $t = 40$ and $t = 80$ are chosen, so we can study the interaction regions without the influence of the boundary. At $t = 40$ and 80, the solution at the interaction region, which is our first focus point, consists a four-sided cell where the stem at the front is bigger but shorter than the stem at the back. The heights of the front wave are about 0.4305 and 0.4372 for $t = 40$ and $t = 80$ (see the last plot in Figure 4) which are larger than double of the initial wave amplitude $A = 0.2$, a property which is often associated with nonlinear interactions. The center cell is qualitatively resembles the solutions observed for KP equation. The size of the

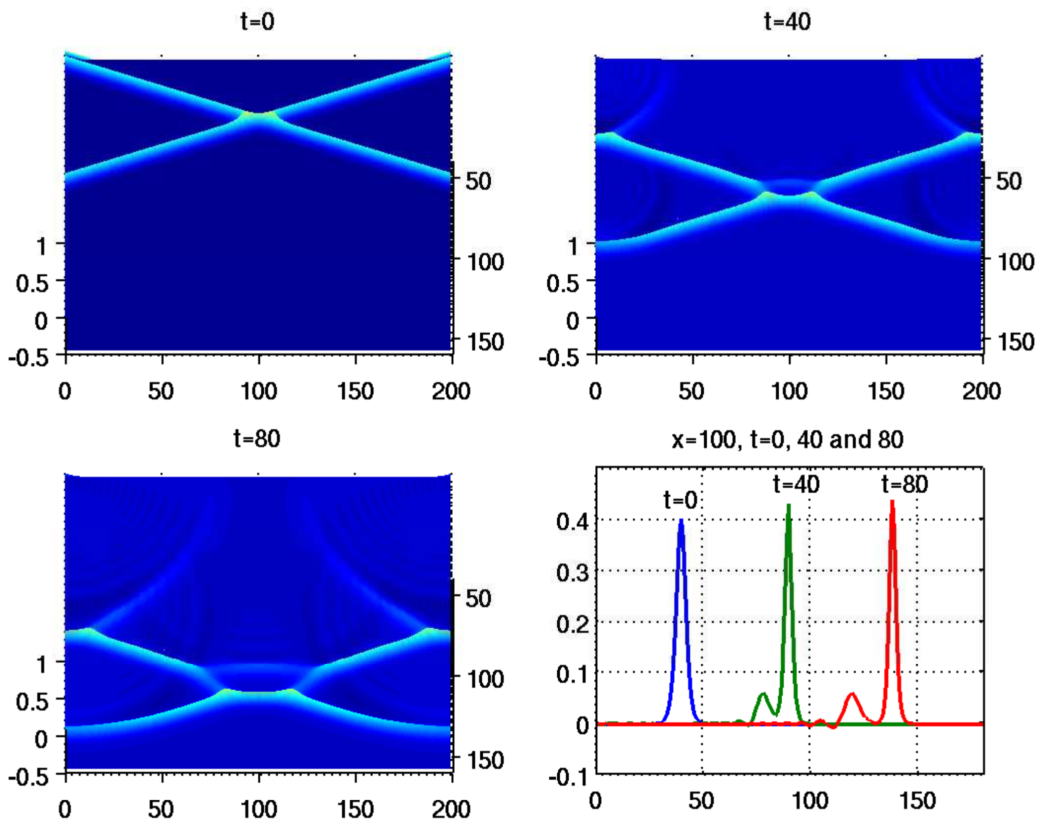

FIGURE 4. Oblique interaction of two solitary waves with amplitude $A = 0.2$ and attack angle $\theta = 40^o$.

center cell increased from $t = 40$ to $t = 80$ and the height of the front waves also increased. Once the waves feel the sides of the wave tank, they will straighten themselves near the sides and at the sides, the wave at the back is bigger. To observe what happens for large t with the influence of the side walls, a larger computational domain was taken to compute the wave profile at $t = 180$ which is plotted in Figure 5. The wave height in the middle (the front wave) is .38, smaller than the corresponding values at $t = 40$ and $t = 80$.

To have a clear view of the functions at the sides of the wave tank, the functions $\eta(0, y, 180)$ and $v(0, y, 180)$ are also plotted in Figure 5 and they are almost indistinguishable from the plots. The horizontal velocity u at the sides is small with the maximum being 0.004, which is what we hoped because its physical implication. In summary, the wave

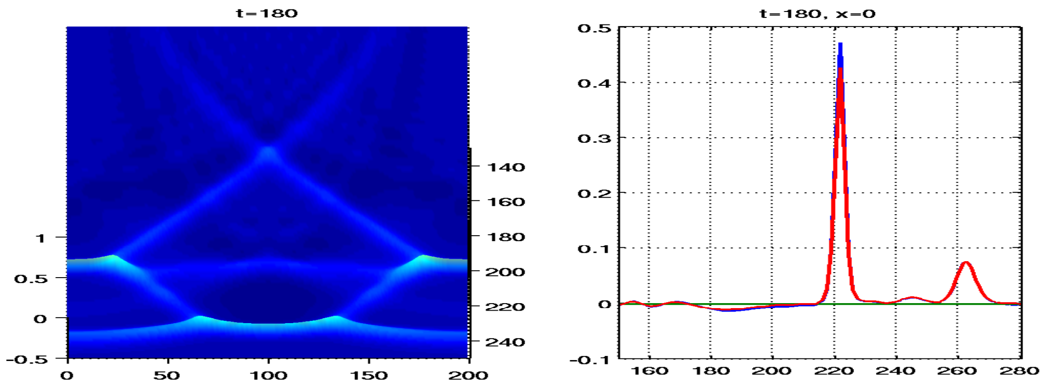

FIGURE 5. Oblique interaction of two solitary waves with amplitude $A = 0.2$ and attack angle $\theta = 40^0$.

profile at $t = 180$ is strongly two-dimensional and very different from what we will observe in the next subsection for the case with $\theta = 10^o$.

3.2. $A = 0.2$ **and** $\theta = 10^o$**.** In this experiment, a much smaller attack angle $\theta = 10^o$ is taken with the amplitude $A = 0.2$ and $y_0 = 15$. The modes in the pseudo-spectral method are taken to be 512 in both directions and the time-step size is 0.025. The surface profiles at $t = 20, 40, 60$ along with their detailed view at $x = 100$, which is at the middle of wave tank in x-direction are plotted in Figure 6. At middle of the tank, instead of a clear four-sided cell, one finds the front wave and the back wave are almost detached. The height of the front wave is much bigger than that of the back wave. The highest point of the front wave is in the middle and moves faster, it will eventually lead the rest of the wave, and therfore the wave front curves up. The reverse is true for the wave at the back and the wave is curves down (see Figure 6 for detail). The height of the front wave starts from double of the initial wave profile which is .4 to higher and then decreases between $t = 20$ to $t = 60$.

Now, with the effect of the boundary, the whole picture of the waves change. Since the middle of the front wave is bigger than its sides, the middle moves faster and the whole front wave curves up, see Figure 7 with $t = 150$ and $t = 200$. In the mean time, the opposite is true for the back wave. At $t = 200$, there is a curved up front wave and also a curved down back wave. But at the sides, the back wave has a bigger amplitude than the front wave. So an interaction of the front and back waves happens during the time $t = 200$ and $t = 240$ near the sides. The separation of the front and back wave is now complete. After that,

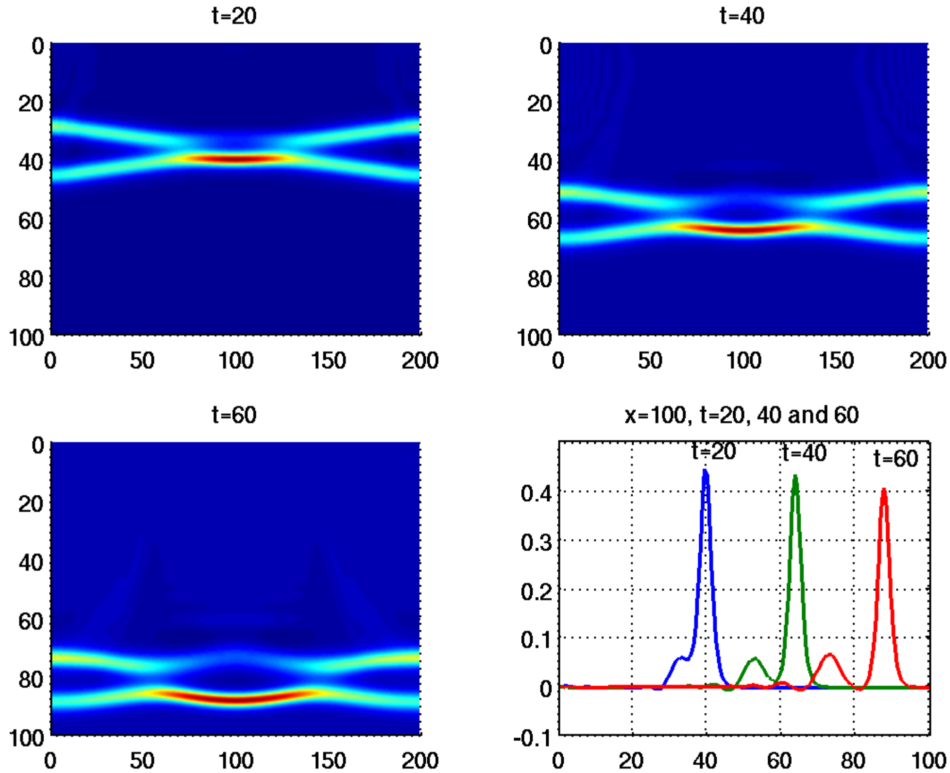

FIGURE 6. Oblique interaction of two solitary waves with amplitude $A = 0.2$ and attack angle $\theta = 10^o$.

both waves move move down and straighten themselves. It might still take some time for them to evolve into two one-dimensional solitary waves, cf. Figure 7.

3.3. $A = 0.2$ **and** $\theta = 90^o$**.** In this case, the center of the interaction does not form a cell. When a large enough computation domain is used, the two waves seems to travel without any changes at the center. In Figure 8, the wave surface profiles at the center with $t = 40$ is plotted to show the phenomena. But when the side walls are involved, the front half of the initial waves is weakened significantly. There is a big reflection about the side walls and the reflective waves have the heights almost the same as the initial waves. The wave surface profiles are plotted in Figure 8. Please note that the two pictures in Figure 8 are from two different computations. For the first one, a very large computation domain is used and only part of the computational domain is plotted to show the interaction zone of the solitary waves without

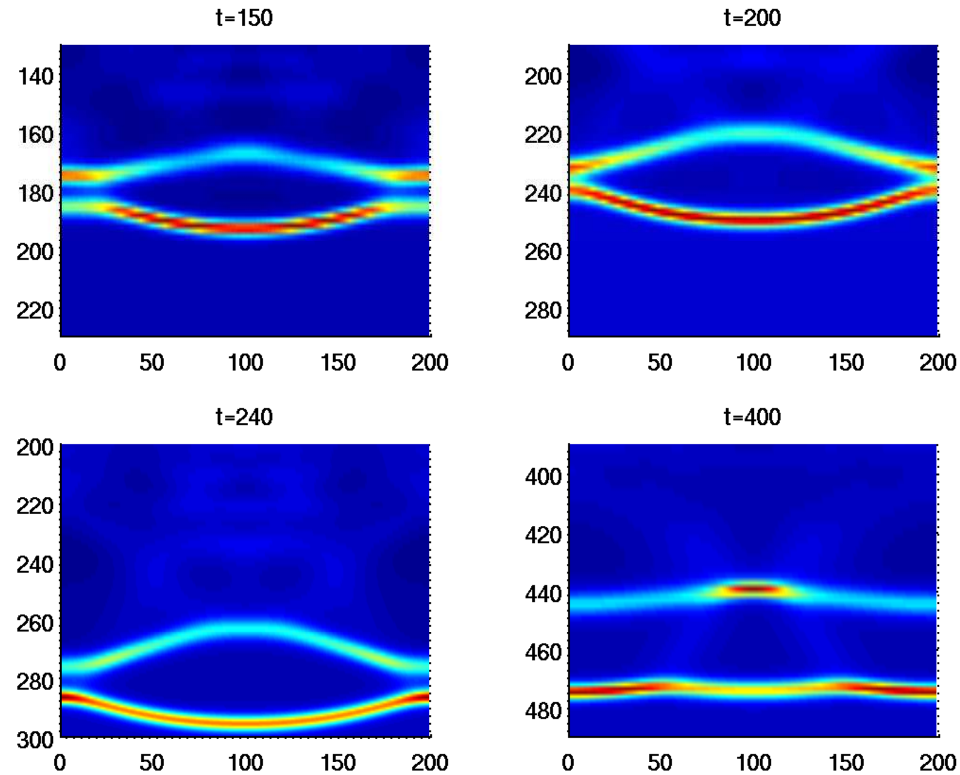

FIGURE 7. Wave surface at $A = 0.2$ and $\theta = 10^o$.

the interference of the boundary. For the second one, the whole picture of the wave profile is presented.

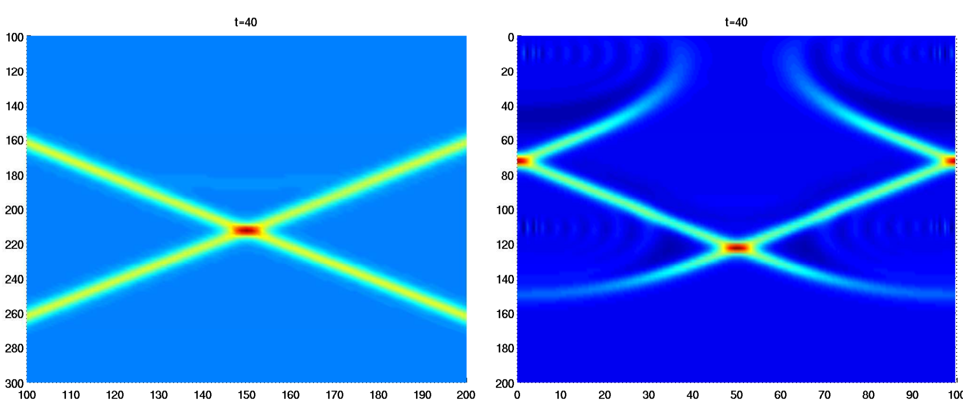

FIGURE 8. Wave surface at $A = 0.2$ and $\theta = 90^o$.

3.4. **A summary.** In general, the oblique interactions of solitary waves have several properties. For the case with attack angle $\theta = 90^o$, the interaction is very weak and two waves seems to travel independently. For the case with $\theta = 40^o$, a center four-sided cell is formed in the middle of the interaction. The front stem is bigger and shorter than the back stem. For the case with $\theta = 10^o$, two almost separated wave are formed. The front one is large and curved up while the back one is weak and curved down. Other numerical experiments are also conducted. The results show that the transition from one scenario to the other is gradual.

References

[1] T. R. Akylas, *Three-dimensional long water-wave phenomena*, in Annual review of fluid mechanics, Vol. 26, Annual Reviews, Palo Alto, CA, 1994, pp. 191–210.

[2] A. A. Alazman, J. P. Albert, J. L. Bona, M. Chen, and J. Wu, *Comparisons between the BBM equation and a Boussinesq system*, Adv. Differential Equations, 11 (2006), pp. 121–166.

[3] J. L. Bona and M. Chen, *A Boussinesq system for two-way propagation of nonlinear dispersive waves*, Physica D, 116 (1998), pp. 191–224.

[4] J. L. Bona, M. Chen, and J.-C. Saut, *Boussinesq equations and other systems for small-amplitude long waves in nonlinear dispersive media I: Derivation and the linear theory*, J. Nonlinear Sci., 12 (2002), pp. 283–318.

[5] ——, *Boussinesq equations and other systems for small-amplitude long waves in nonlinear dispersive media II: Nonlinear theory*, Nonlinearity, 17 (2004), pp. 925–952.

[6] J. L. Bona, T. Colin, and D. Lannes, *Long wave approximations for water waves*, Arch. Ration. Mech. Anal., 178 (2005), pp. 373–410.

[7] J. V. Boussinesq, *Théorie générale des mouvements qui sont propagés dans un canal rectangulaire horizontal*, C. R. Acad. Sci. Paris, 73 (1871), pp. 256–260.

[8] M. Chen, *Equations for bi-directional waves over an uneven bottom*, Mathematics and Computers in Simulation, 62 (2003), pp. 3–9.

[9] ——, *From boussinesq systems to kp-type equations*, Canadian Applied Mathematics Quarterly, 15 (2007).

[10] ——, *Numerical investigation of a two-dimensional boussinesq system*, Discrete and Continuous Dynamical Systems, 23 (2009), pp. 1169–1190.

[11] M. Chen and G. Iooss, *Periodic Wave Patterns of two-dimensional Boussinesq systems*, European Journal of Mechanics B/Fluids, 25 (2006), pp. 393–405.

[12] ——, *Asymmetrical Periodic Wave Patterns of two-dimensional Boussinesq systems*, Physica D., 237 (2008), pp. 1539–1552.

[13] P. Daripa and R. K. Dash, *A class of model equations for bi-directional propagation of capillary-gravity waves*, Internat. J. Engrg. Sci., 41 (2003), pp. 201–218.

[14] B. B. Kadomtsev and V. I. Petviashvili, *On the stability of solitary waves in weakly dispersing media*, Sov. Phys. Dokl., 15 (1970), pp. 539–541.

[15] C. Katsis and T. R. Akylas, *On the excitation of long nonlinear water waves by a moving pressure distribution. Part 2. Three-dimensional effects.*, J. Fluid Mech., 177 (1987), pp. 49–65.

[16] D. H. Peregrine, *Equations for water waves and the approximation behind them*, in Waves on beaches and resulting sediment transport; proceedings of an advanced seminar conducted by the Mathematics Research Center, Univ. Wisconsin, Academic Press: New York, 1972, pp. 95–121.